

Covalent organic frameworks for direct photosynthesis of hydrogen peroxide from water, air and sunlight

Received: 21 November 2022

Accepted: 6 July 2023

Published online: 19 July 2023

Check for updates

Fuyang Liu^{1,2,3,7}, Peng Zhou^{4,7}, Yanghui Hou^{1,2,3}, Hao Tan⁵, Yin Liang⁵, Jialiang Liang⁶, Qing Zhang⁵, Shaojun Guo⁵, Meiping Tong^{1,2,3}✉ & Jinren Ni^{1,2,3}

Solar-driven photosynthesis is a sustainable process for the production of hydrogen peroxide, the efficiency of which is plagued by side reactions. Metal-free covalent organic frameworks (COFs) that can form suitable intermediates and inhibit side reactions show great promise to photo-synthesize H₂O₂. However, the insufficient formation and separation/transfer of photo-generated charges in such materials restricts the efficiency of H₂O₂ production. Herein, we provide a strategy for the design of donor-acceptor COFs to greatly boost H₂O₂ photosynthesis. We demonstrate that the optimal intramolecular polarity of COFs, achieved by using suitable amounts of phenyl groups as electron donors, can maximize the free charge generation, which leads to high H₂O₂ yield rates (605 μmol g⁻¹ h⁻¹) from water, oxygen and visible light without sacrificial agents. Combining in-situ characterization with computational calculations, we describe how the triazine N-sites with optimal N 2p states play a crucial role in H₂O activation and selective oxidation into H₂O₂. We further experimentally demonstrate that H₂O₂ can be efficiently produced in tap, river or sea water with natural sunlight and air for water decontamination.

As a versatile reagent, hydrogen peroxide (H₂O₂) is widely used in the fields of chemical synthesis, energy storage and water treatment^{1,2}. At present, oxidation of anthraquinone, electrochemical synthesis, and noble metal catalysis are the common methods used to produce H₂O₂^{2,3}. However, these methods require high energy input and cause environmental pollution by the release of toxic by-products^{4,5}. Due to the use of naturally abundant water and oxygen in air as raw materials and solar light as energy input, H₂O₂ photosynthesis, especially without using sacrificial agents, is regarded as one of the green and sustainable methods, which yet is plagued by the severe side reactions such as the decomposition of produced H₂O₂ into oxygen and water

due to the metastable feature of H₂O₂ during the synthesis process^{6–12}. As one type of novel metal-free crystalline polymers that can form suitable intermediates and inhibit side reactions for H₂O₂ generation, covalent organic frameworks (COFs) recently show great promise in the field of H₂O₂ photosynthesis^{13,14}. The insufficient formation or separation of excitons (bound state of electron–hole pairs) for the free charge generation in COFs yet seriously constrains the high-efficiency of H₂O₂ photocatalytic generation^{15,16}. Some interfacial modulating strategies such as constructing heterojunction¹⁷ and incorporating single atoms¹⁸ are beneficial for enhancing the photoexcitation and charge separation/transfer of COFs photocatalysts, which yet require

¹College of Environmental Sciences and Engineering, Peking University, Beijing 100871, PR China. ²The Key Laboratory of Water and Sediment Sciences (Ministry of Education), Peking University, Beijing 100871, PR China. ³State Environmental Protection Key Laboratory of All Material Fluxes in River Ecosystems, Peking University, Beijing 100871, PR China. ⁴School of Environment and Energy, Peking University Shenzhen Graduate School, Shenzhen, Guangdong 518055, PR China. ⁵School of Materials Science and Engineering, Peking University, Beijing 100871, PR China. ⁶College of Environment and Ecology, Chongqing University, Chongqing 400045, PR China. ⁷These authors contributed equally: Fuyang Liu, Peng Zhou. ✉e-mail: tongmeiping@pku.edu.cn

multistep, complex and time/energy-consuming synthesis process. Hence, developing a facile and cost-effective strategy to improve the generation and separation of photogenerated charges without introducing severe side reactions is in great demand for H₂O₂ photo-synthesis, yet remains a great challenge.

Herein, we provide a facile and economical strategy for the design of metal-free donor-acceptor (D-A)-type COFs with optimal intramolecular polarity by introducing suitable amounts of phenyl groups as electron donors for excitonic regulation to boost the direct photocatalytic H₂O₂ production from water, air and sunlight without using sacrificial agent. By using triazine-cored triamine with different amounts of phenyl groups ($n = 0, 1, 2$) as the precursors, a class of D-A COFs with different intramolecular polarity were successfully synthesized. We find that weak intramolecular polarity in D-A COFs constrains excitons dissociation, yet too strong intramolecular polarity inhibits excitons formation via weakened π -conjugated effect as well as decreases the photo-stability of COFs. The well-designed COFs with the optimal intramolecular polarity (named as COF-N32) can facilitate excitons formation and dissociation, leading to the high and stable H₂O₂ yield (605 $\mu\text{mol g}^{-1} \text{h}^{-1}$) with solar-to-chemical efficiency of 0.31% in water without additional sacrificial reagent. COF-N32 can also efficiently produce H₂O₂ in real water samples including tap water, river water and sea water even with natural solar light irradiation. Moreover, COF-N32 can be assembled into practical devices for facile consecutive uses with high photocatalytic stability under natural solar irradiation. In addition, we demonstrate that the produced H₂O₂ aqueous solution (without further separation) can be directly employed in water decontamination, indicating the potential application feasibility of COF-N32. Via in-situ Fourier transform infrared (FTIR) characterization and density functional theory (DFT) calculation, we reveal that the suitable N $2p$ states and C $2p$ states in COF-N32 with optimal intramolecular polarity effectively reduce the energy barrier for H₂O activation and oxygen reduction, respectively, contributing to the high efficiency.

Results and discussion

Characterization of synthesized COFs

The COFs photocatalysts were synthesized by a solvothermal method. Figure 1a illustrates the theoretical chemical structures of three triazine-based COFs, which is also confirmed by the corresponding solid state ¹³C nuclear magnetic resonance (NMR) spectra (Fig. 1b). Clear peaks at -180 ppm, -170 ppm, -145 ppm and -115 ppm in the ¹³C NMR spectra of three COFs can be attributed to carbonyl carbon, triazine carbon, C-NH (amine linkage) carbon and olefin carbon, respectively¹⁹. The stretching vibration bands of C=C bond at -1573 cm⁻¹ and C-N bond at 1255 cm⁻¹ in the FTIR spectra of three COFs (Fig. 1c) suggest the occurrence of Schiff base reaction and enol-to-keto tautomerism during the fabrication process of three COFs^{19,20}. The formation of carbonyl group and amine linkage in three COFs is further confirmed by X-ray photoelectron spectroscopy (XPS) analysis (Fig. S1). Based on the simulation and Pawley refinement, the obvious peaks at $2\theta = 9.6^\circ$, 5.5° and 3.9° corresponding to (100) planes and $2\theta = -27^\circ$ corresponding to (002) planes in the X-ray diffraction (XRD) pattern (Figure S2) suggest that three COFs contain crystalline structure^{20–22}. Scanning electron microscopy (SEM) and transmission electron microscopy (TEM) images show that the three COFs are tiny granular particles with diameter of 2–3 μm , which are assembled by numerous nanorods (Figs. S3 and S4). The above results confirm the successful fabrication of three COFs.

To explore whether the incorporated phenyl group on triazine rings would affect the formation and separation of excitons in COFs, the intramolecular polarity of electronic structure in three COFs was determined. The theoretical calculation of charge distribution indicates that in the hexatomic rings (one type of octupolar subunit), carbonyl group with *meta* position acts as electron acceptor, while

olefin group serves as donor (Figs. 1d and S5)^{23–25}. For another type of octupolar subunit, due to the well-delocalizing π -electron over the three aromatic carbon atoms, 1,3,5-triazine ring with electron deficiency in all three COFs can also serve as electron acceptor center^{26,27}. While enamine group in three COFs as well as phenyl group in COF-N32 and COF-N33 can act as electron-donating groups^{28,29}. Clearly, all three COFs contain octupolar conjugated structure with two subunits (Fig. 1e), which is expected to facilitate the efficient charge separation especially in each subunit coupling with appropriate intramolecular polarity²⁷. Accordingly, stable radicals with strong signal intensities are observed in the solid-state electron spin resonance (ESR) spectra of three COFs under dark condition at room temperature (Fig. S6). The paramagnetic absorption signal intensities of three COFs follow the order of COF-N31 > COF-N32 > COF-N33 (Fig. S6), indicating that different amounts of unpaired electrons exist in three D-A COFs under dark condition³⁰. With increasing amount of phenyl groups as electron donors from 0 (COF-N31) to 1 (COF-N32) and further to 2 (COF-N33), the intramolecular polarization of composition fragments in three COFs decrease from 0.072 e \AA^{-1} for COF-N31 to 0.032 e \AA^{-1} for COF-N32 and further to 0.020 e \AA^{-1} for COF-N33 (Fig. S7 and Table S1). The direction of intramolecular polarity in these COFs is from enamine and/or benzene groups to triazine groups (Fig. S7). Furthermore, the molecular polarity index (MPI) also follows the same order of COF-N31 (0.53 eV) > COF-N32 (0.50 eV) > COF-N33 (0.48 eV) (Table S2).

The solvatochromic behaviors of COFs were employed to further determine their polar properties. Obvious shift of emission peaks (-48 nm) is observed in fluorescence spectra of COF-N31 dispersed in water (as a polar solvent) relative to those in methanol, dichloromethane and ethyl acetate (with weaker polarity than water), indicating the strong local dipolar nature of COF-N31 with weak electron donor in π -conjugated system³¹. Similar observation has also been previously reported for COFs with high polarity^{27,32}. In contrast, for both COF-N32 and COF-N33, relatively smaller positive shifts of emission peaks (<25 nm) are observed in water relative to other organic solvents (Fig. S8). The weak solvatochromic behaviors of both COF-N32 and COF-N33 can be attributed to the sufficient electron donor with phenyl or diphenyl group in the octupolar π -conjugated framework. The COFs with higher polarity usually exhibit higher affinity to polar H₂O³³. Note the intramolecular polarity follows the order of COF-N31 > COF-N32 > COF-N33. Accordingly, the contact angle of three COFs follows the order of COF-N31 (121°) < COF-N32 (139°) < COF-N33 (145°) (Fig. S9). Meanwhile, the unit water adsorption capacity is also consistent with the order of COF-N31 > COF-N32 > COF-N33 (Fig. S10).

In general, the excessively strong intramolecular polarity in COFs would restrain the π conjugated effect in sp^2 -hybridized orbit structure of COFs, leading to the inhibition of electron excitation^{34,35}. The O atom with high electronegativity in COF-N31 with strong polarity can attract electrons surrounding amine N atoms, the delocalization on triazine rings in the lowest unoccupied molecular orbital (LUMO) of COF-N31 thus is limited across three atoms (N and C atoms) in each direction (Fig. S11a). In contrast, due to the less polarity relative to COF-N31, LUMO of COF-N32 and COF-N33 can be well delocalized across nine atoms surrounding the triazine rings (Figs. S11b and S11c), indicating the enhanced π conjugation in COF-N32 and COF-N33. This would facilitate the excitation of electrons in these two COFs under light irradiation. The less intramolecular polarity of COFs has shown to result in the overlap of the highest occupied molecular orbital (HOMO) and LUMO^{36,37}. Similarly, for COF-N32 and COF-N33 with less polarity, the overlap of HOMO and LUMO especially on the C atoms in keto structure and diphenyl group is also observed (Fig. S11). S_m index (parameter denoting the hole-electron recombination degree³⁸) of three COFs in the excited state based on DFT calculation is found to follow the order of COF-N31 (0.33) < COF-N32 (0.36) < COF-N33 (0.38) (Table S2). The observation indicates that hole-electron in COF-N32 and COF-N33 is

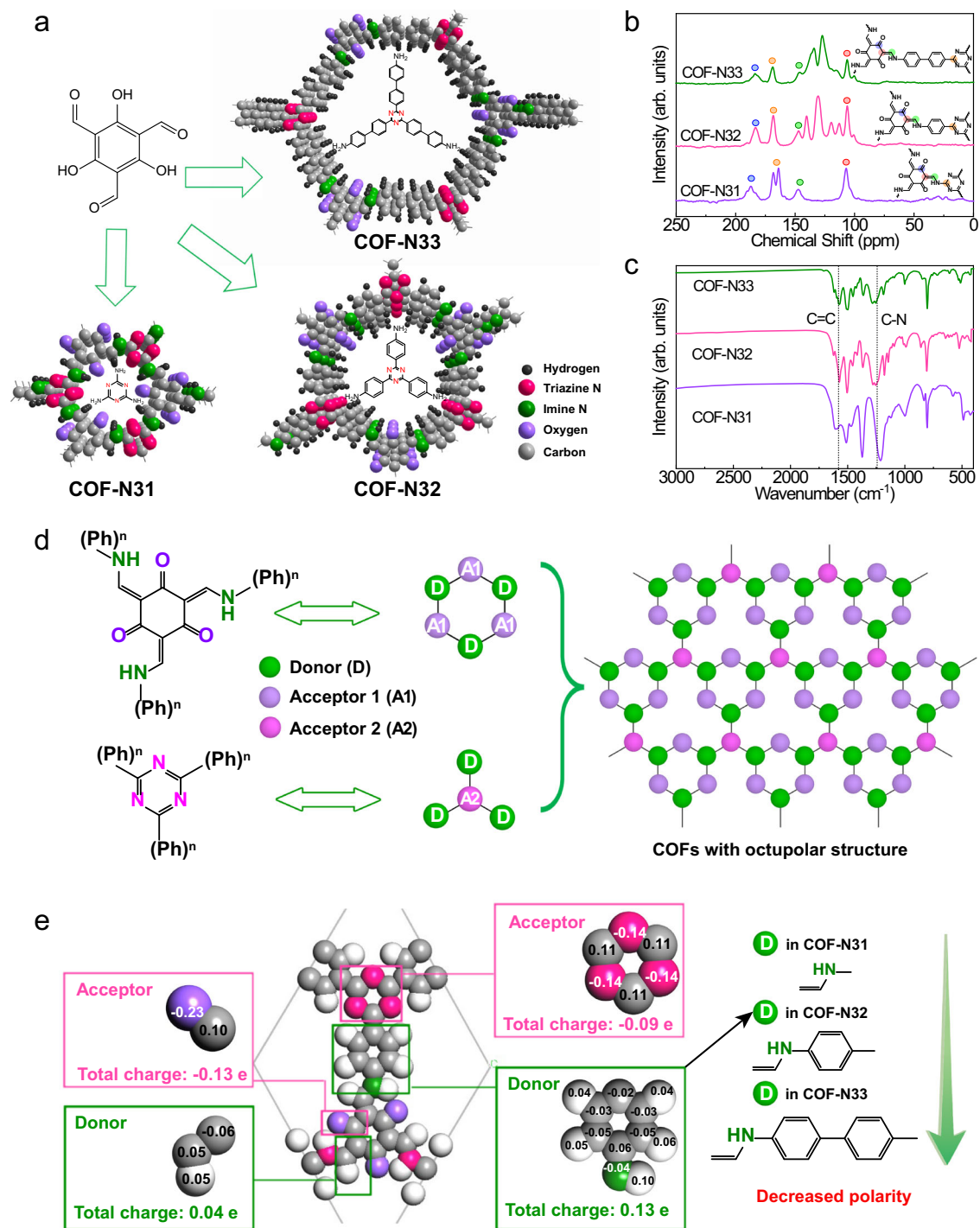


Fig. 1 | Chemical structure. **a** Schematic illustration of synthesis process of COF-N31, COF-N32 and COF-N33. **b** ^{13}C nuclear magnetic resonance (NMR) spectra and **c** Fourier transform infrared spectroscopy (FTIR) of COF-N31, COF-N32 and COF-

N33. **d** The schematic illustration of the octupolar structure in COF-N31, COF-N32 and COF-N33. **e** DFT calculation on charge distribution of COF-N32 structure.

relatively readily to be recombined than COF-N31. Overall, the strong intramolecular polarity in COF-N31 theoretically inhibits the π -conjugation, the subsequent excitation of electrons, as well as the recombination of charges. In contrast, the weak polarity in COF-N33 yet facilitates the π -conjugated effect, the excitation of electrons, and charge recombination. COF-N32 with moderate polarity among three COFs is expected to display the best photocatalytic property.

The formation, transfer and separation of photo-induced excitons in three COFs were investigated. Tauc plot based on UV-vis diffused reflectance spectra (DRS) reveals that all three COFs exhibit $n-\pi^*$

transition in N atoms³⁹, while COF-N33 with more benzene units also contains more obvious signals of $\pi-\pi^*$ transition⁴⁰. The band gaps of COF-N31 (2.72 eV) > COF-N32 (2.42 eV) > COF-N33 (2.40 eV) (Fig. 2a) are also consistent with the results of calculated ones (Fig. S12). The observation indicates that COF-N32 and COF-N33 exhibit higher light absorption efficiency relative to COF-N31, which can be attributed to the efficient π -conjugated effect with relatively weaker intramolecular polarity of these two COFs than that of COF-N31²⁷. The results of electrical impedance spectra (EIS) indicate that COF-N32 and COF-N33 have relatively smaller charge transfer resistance than COF-N31

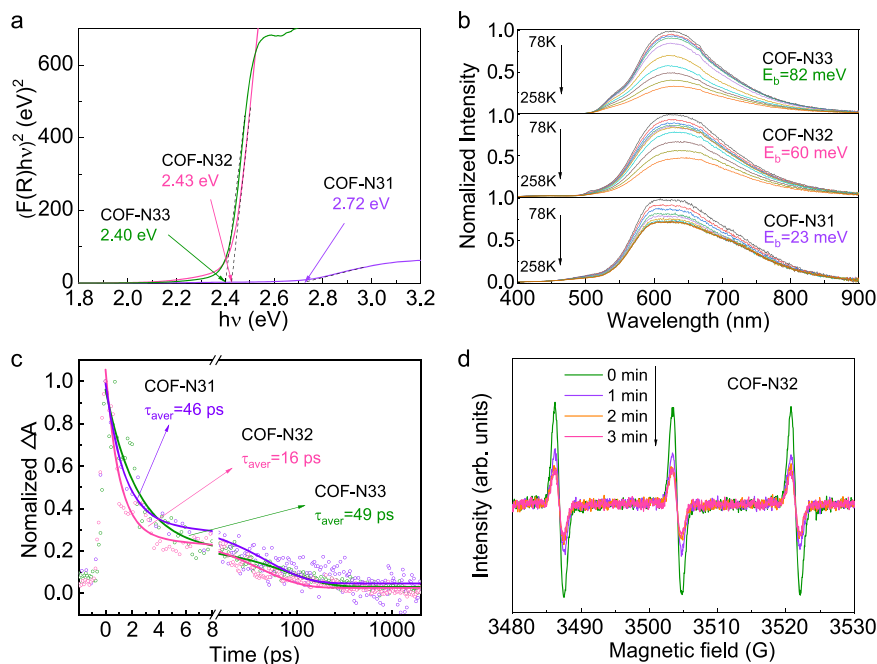


Fig. 2 | Polarity property. **a** Tauc plot of three COFs; **b** Temperature-dependent PL spectra of three COFs excited at 365 nm for the determination of binding energy (E_b). **c** Photoinduced absorption decay dynamics of three COFs with the excitation

of 360 nm pump pulse ($P = 4.3 \text{ mJ cm}^{-2}$ per pulse); **d** The signal intensity of 2,2,6,6-tetramethyl-1-piperidinyloxy (TEMPO) for charge detection in COF-N32 under light irradiation.

(Fig. S13), contributing to the efficient interfacial electron transfer speed of these two COFs. The observation agrees with the efficient π -conjugation through electronic push-pull effect in COF-N32 and COF-N33 due to their relatively weaker intramolecular polarity discussed above. Both the exciton binding energy (E_b) determined by temperature-dependent photoluminescence (PL) spectra and the emission peaks intensities in steady-state PL spectra of three COFs follow the order of COF-N33 > COF-N32 > COF-N31 (Figs. 2b, S14 and S15), indicating that the dissociation of formed excitons in three COFs is in the order of COF-N31 > COF-N32 > COF-N33.

The transient absorption (TA) was performed to analyze charge carrier dynamics in three COFs. The broad and positive absorbance changes (ΔA) observed around 500–700 nm can be attributed to the photoinduced absorption of photoexcited electrons in the conduction band (CB) of three COFs (Fig. S16)^{41,42}. Among three COFs, photoexcited electrons in COF-N32 exhibits smaller average lifetime (16 ps) relative to those in COF-N31 (46 ps) and COF-N33 (49 ps) (Fig. 2c), which is consistent with the average lifetimes obtained in PL decay curves in the nanosecond domain (0.31 ns for COF-N32 relative to 0.75 ns for COF-N31 and 1.34 ns for COF-N33) (Fig. S17). The observations suggest the more prominent non-radiative rate in COF-N32 than COF-N31 and COF-N33^{27,43}. ESR analysis (Fig. 2d) shows that under visible light irradiation, COF-N32 can generate more photo-induced free charges (via the excitons formation and dissociation) than COF-N31 (Fig. S18a) and COF-N33 (Fig. S18b). The generation of photo-induced free charges in COF-N32 is confirmed by detecting the reduction product tetramethylpiperidine (TEMP, m/z 142.15826, ESI⁺) via reaction of electrons and 2,2,6,6-tetramethyl-1-piperidinyloxy (TEMPO) (Fig. S19). The above results show that among all three COFs, COF-N32 with moderate intramolecular polarity in the octupolar conjugated structure can generate the greatest amount of charges (i.e. electrons and holes) under visible light irradiation (Eq. S4). The energy band positions of three COFs derived from XPS valence band spectra combined with Tauc plot indicate the thermodynamic feasibility of oxygen reduction reaction (ORR) to photosynthesize H_2O_2 (-0.33 V vs. NHE) by three COFs (-1.09 V vs. NHE for COF-N31, -0.55 V vs. NHE for COF-N32 and -0.48 V vs. NHE for COF-N33) (Figs. S20 and S21)⁸, while

the two-electron water oxidation reaction (WOR) directly to H_2O_2 (1.77 V vs. NHE) is thermodynamically feasible by COF-N32 (1.88 V vs. NHE) and COF-N33 (1.92 V vs. NHE) but not by COF-N31 (1.63 V vs. NHE) (further discussion is provided below).

Photocatalytic H_2O_2 production by COFs

The photosynthesis of H_2O_2 by COFs was evaluated in pure water without using any sacrificial agent under visible light irradiation ($\lambda > 420 \text{ nm}$, 100 mW cm^{-2}). During 12 h reaction duration, COF-N32 with moderate intramolecular polarity in the octupolar conjugated structure exhibits significantly improved performance for H_2O_2 photosynthesis relative to COF-N31 (with strong intramolecular polarity) and COF-N33 (with weak intramolecular polarity). Specifically, after 12 h of visible light irradiation, H_2O_2 yield by COF-N32 reaches $7092 \mu\text{mol g}^{-1}$ ($605 \mu\text{mol g}^{-1} \text{ h}^{-1}$), which is greatly higher than that by COF-N31 ($4316 \mu\text{mol g}^{-1}$, $442 \mu\text{mol g}^{-1} \text{ h}^{-1}$) and COF-N33 ($1736 \mu\text{mol g}^{-1}$, $155 \mu\text{mol g}^{-1} \text{ h}^{-1}$) (Figs. 3a and S22). Negligible amount of H_2O_2 (<5%) could be degraded by metal-free COF-N32 under visible light irradiation (Fig. S23), indicating the inhibited side reaction. This contributes to the stable and high yield of H_2O_2 in water by COF-N32. H_2O_2 yields by COF-N32 is also higher than those by conventional photocatalysts including TiO_2 , $\text{g-C}_3\text{N}_4$ and WO_3 (Figs. 3a and S22). Moreover, COF-N32 can yield over $3.17 \text{ mmol g}^{-1} \text{ h}^{-1}$ with the addition of 1 mg COF-N32 in 50 mL ultrapure water after 3 h of visible light irradiation (Fig. S24), which is much higher than those of recently reported photocatalysts in pure water under similar measurement conditions (Fig. 3b and Table S3). In addition, COF-N32 exhibits high apparent quantum yield (AQY) of 6.2% at 459 nm (Fig. 3c). The solar-to-chemical efficiency of COF-N32 (0.31%) under visible light irradiation (details are provided in Supporting information) is greatly higher than solar-to-biomass efficiency by plants ($\sim 0.1\%$).

Due to the inhibited side reaction, COF-N32 also exhibits stable H_2O_2 yield and excellent reusability for 5 reused cycles (Fig. 3d). No obvious structural change is observed in COF-N32 after use (Fig. S25), indicating its excellent photo-stability under visible light irradiation. The stable H_2O_2 yield during the 5 reused cycles and no obvious change of crystalline structure after use are also achieved for COF-N33

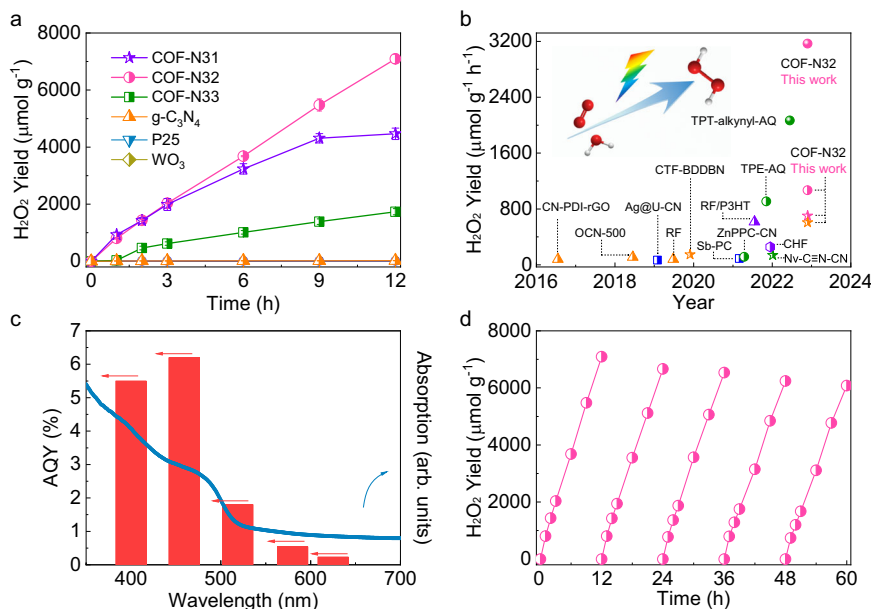


Fig. 3 | Photocatalytic performance. **a** Photosynthesis of H₂O₂ by COF-N31, COF-N32 and COF-N33. Experimental conditions: $\lambda > 420$ nm (298 K; xenon lamp, light intensity: 100 mW cm⁻²), ultrapure water (50 mL), photocatalyst (25 mg). **b** The comparison of H₂O₂ photosynthesis rate by COF-N32 with other reported photocatalysts without sacrificial agent under the similar measurement conditions (shape of symbol refers to the dosage of photocatalysts, sphere: 1 mg; circle: 10 mg; star: 20–30 mg; triangle: 50 mg; square: 100 mg; hexagon: 375 mg; color of symbol

refers to the reaction duration, green: 1 h; blue: 1.2–2 h; pink: 3 h; purple: 6 h; orange: 10–24 h). **c** The apparent quantum yield (AQY) of COF-N32 as a function of wavelength (purple light at 400 nm, blue light at 459 nm, green light at 519 nm, yellow light at 580 nm, red light at 625 nm). **d** The reusability of COF-N32 for H₂O₂ photosynthesis. Experimental conditions: $\lambda > 420$ nm (298 K; xenon lamp, light intensity: 100 mW cm⁻²), ultrapure water (50 mL), photocatalyst (25 mg). Error bars in **a** represent the average values (mean \pm s.d., $n = 3$).

(Figs. S26a and S26b). In contrast, the H₂O₂ yield by COF-N31 dramatically decreases with increasing reused cycles (Fig. S26c), indicating the relatively low photo-stability of COF-N31 during the reaction duration. The decreased crystallinity of COF-N31 after photocatalytic reaction (Fig. S26d) confirms its low photo-stability during the reaction process. The photo-stability observed for both COF-N32 and COF-N33 during the reaction duration indicates that h^+ generated by COF-N32 and COF-N33 directly oxidizes water to H₂O₂ instead of attacking COFs. The WOR directly to H₂O₂ by COF-N32 and COF-N33 (thermodynamically feasible stated above, Fig. S21) is confirmed by isotopic experiments using H₂¹⁸O and ¹⁶O₂ as precursors in a sealed reactor (Figs. S27b and S27c). Unlike that obtained for COF-N32 and COF-N33 (two COFs with relatively weak intramolecular polarity), WOR directly to H₂O₂ by COF-N31 with strong intramolecular polarity yet is not thermodynamically feasible (Fig. S21), which is also confirmed by isotopic experiments (Fig. S27a). Instead, h^+ generated by COF-N31 can attack COF itself, leading to the low photo-stability of COF-N31 during the reaction duration. Note the quench of h^+ by COF-N31 can promote the separation of e^-h^+ pairs, which is beneficial for the H₂O₂ production^{44,45}. Therefore, even though the amount of free charges (i.e. e^- and h^+) by COF-N31 is much lower than that by COF-N32 (Figs. S18a and 2d), H₂O₂ production rate by COF-N31 is similar to that by COF-N32 at the beginning of photocatalytic process (Fig. 3a). The decreased H₂O₂ production rate observed with the increasing reaction duration can be attributed to the self-decomposition of COF-N31 during the reaction duration, which is also confirmed by the decreased crystallinity of COF-N31 after photocatalytic reaction (Fig. S26d). Similar observation about self-decomposition of COFs during H₂O₂ photosynthesis in water has also been reported previously⁴⁶. The results clearly show that in pure water, COF-N31 with strong intramolecular polarity has low photo-stability of COF-N31 during the reaction duration, whereas COF-N32 and COF-N33 with relatively weak intramolecular polarity especially COF-N32 owns excellent photo-stability under visible light irradiation and can be consecutively reused for the photo-generation of H₂O₂.

The H₂O₂ yield (~3.5 mM) by COF-N32 after 12 h with visible light irradiation (Fig. 3a) can meet the H₂O₂ concentration required for water purification⁴⁷. The filtrate of H₂O₂ generated by COF-N32 can be directly used to efficiently inactivate antibiotic resistant bacteria under dark condition, indicating that the produced H₂O₂ can be employed for water disinfection (Fig. S28). In addition to ex-situ disinfection, COF-N32 can also in-situ disinfect antibiotic resistant bacteria and degrade organic pollutant with emerging concerns (diclofenac) under visible light irradiation (Fig. S29). More importantly, COF-N32 is able to produce H₂O₂ at wide ranges of initial solution pH (3–11) (Fig. S30). Due to the consumption of radicals by dissolving ions and natural organic matter (NOM), the H₂O₂ production in real waters has been previously found to be inhibited^{48,49}. However, we experimentally demonstrate that the efficient H₂O₂ photosynthesis by COF-N32 can also be achieved in more available real water samples with complex water matrix conditions. The H₂O₂ photosynthesis rate by COF-N32 reaches 667, 648 and 554 $\mu\text{mol g}^{-1} \text{h}^{-1}$ in tap water, river water and sea water within 3 h of visible light irradiation, respectively (Fig. S31). The H₂O₂ photosynthesis in a cheap commercial membrane filter reactor (facile for separation of COF-N32 after use) was also investigated under simulated visible light irradiation. Regardless without or with using rubber plug to prevent the penetration of water through membrane in reactor under gravity, COF-N32 can efficiently produce ~30 $\mu\text{mol H}_2\text{O}_2$ in 2 h for the successive four cycles (Fig. S32).

The H₂O₂ photosynthesis by COF-N32 was further examined under natural sunlight irradiation (Figs. 4a–d). In two different reactor systems (double-walled beaker and membrane filter reactor), COF-N32 can efficiently produce H₂O₂ in different types of water samples under natural sunlight both in cloudy and sunny days (Figs. 4a, c, d, and S33–35). Although the used COF-N32 can be easily recovered by membrane filtration in double-walled beaker or can be separated in membrane filter reactor with the removal of H₂O₂ solution under gravity, COF-N32 powders were immobilized onto indium tin oxide (ITO) glass slide to further ease its recovery and reuse for practical

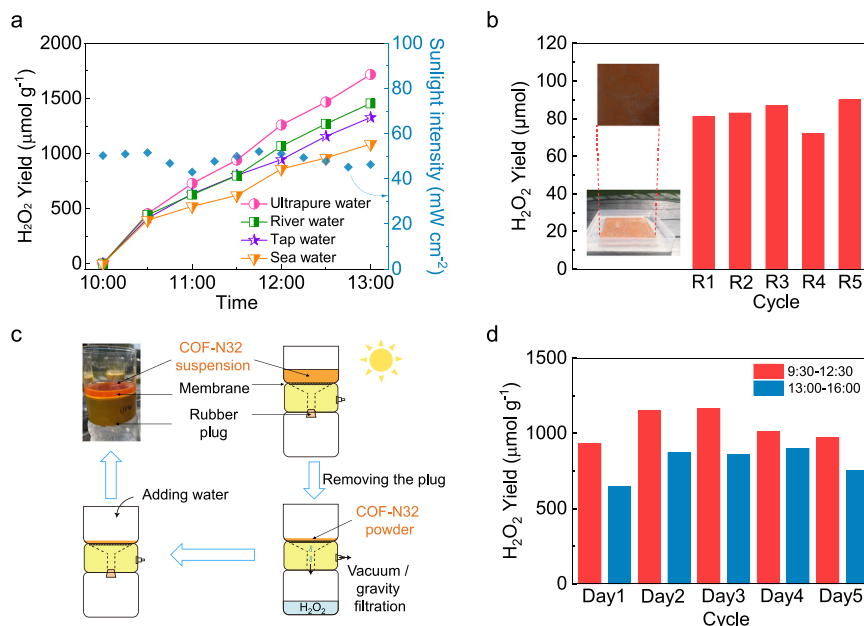


Fig. 4 | Feasibility investigation for practical applications. **a** Photocatalytic H_2O_2 production by COF-N32 in 50 mL of ultrapure water, tap water, river water and sea water under natural sunlight irradiation on a sunny day. **b** Immobilization of COF-N32 powders (60 mg) onto ITO glass slide ($10\text{ cm} \times 10\text{ cm}$) for H_2O_2 production in 200 mL of pure water under natural sunlight irradiation from 10:30 to 13:30 on

sunny days. **c** The schematic illustration of H_2O_2 photosynthesis process in a membrane reactor. **d** The photocatalytic production of H_2O_2 by COF-N32 in a membrane reactor under natural sunlight irradiation. Experimental conditions: ultrapure water (50 mL), photocatalyst (25 mg).

application (Fig. 4b). Pre-experiments show that $\sim 3.5\ \mu\text{mol}$ of H_2O_2 can be produced in every 2 h for the consecutive five cycles by COF-N32-immobilized glass slide ($2\text{ cm} \times 2\text{ cm}$, containing 5 mg COF-N32) under visible light irradiation (Fig. S36). In a scaled-up reactor with working volume of 200 mL, $\sim 85\ \mu\text{mol}$ of H_2O_2 can be generated in 3 h on five sunny days by a larger COF-N32-loaded glass side ($10\text{ cm} \times 10\text{ cm}$ glass slide with the loading of 60 mg COF-N32) under natural sunlight irradiation (Fig. 4b). The results suggest the feasibility of panel-level H_2O_2 photosynthesis based on COFs photocatalysts.

Photocatalytic mechanisms of COFs

The generation process of H_2O_2 by COF-N32 under visible light irradiation was investigated by quenching experiments and in-situ ESR analysis. Negligible H_2O_2 is generated within 12 h when dissolved O_2 in water is eliminated by N_2 purging (Figs. S5a and S37), indicating O_2 is essential for H_2O_2 production. Rotating ring-disk electrode (RRDE) analysis shows that the number of electrons transferred from COF-N32 to O_2 is estimated to be 2.17 (Fig. S38), indicating that O_2 is generally reduced to generate H_2O_2 via the apparent 2-electron reaction. The intermediates during oxygen reduction were further investigated by the trapping experiments. The addition of *p*-benzoquinone (*p*-BQ, the scavenger of $\cdot\text{O}_2^-$) into reaction system significantly inhibits the production of H_2O_2 with negligible yield, suggesting $\cdot\text{O}_2^-$ is an intermediate product crucial for the H_2O_2 photosynthesis. Note that $\cdot\text{O}_2^-$ is the reduction product of O_2 by electrons (e^-) photo-generated by COFs (Eq. S5). As stated above, among three COFs, the amount of e^- generated by COF-N32 is the largest (Fig. 2d). The DMPO- $\cdot\text{O}_2^-$ intensity in the in-situ ESR spectra for COF-N32 thus is higher than the other two COFs (Fig. S39). This indicates that regardless the amount of O_2 adsorbed by COF-N32 was not the highest among three COFs (Figs. S40 and S41), the electron transfer efficiency from COF-N32 to O_2 for the production of $\cdot\text{O}_2^-$ species was higher than the other two COFs. Accordingly, the H_2O_2 yield by COF-N32 is the highest among three COFs. As mentioned above, e^- generated from the dissociation of formed excitons by COFs with light irradiation can react with O_2 to produce $\cdot\text{O}_2^-$ and subsequently to

H_2O_2 (Eqs. S5 and S6). h^+ generated from the separation of e^- - h^+ pairs (excitons) yet can oxidize H_2O to form adsorbed $\cdot\text{OH}$ (Eq. S7) and then to H_2O_2 (Eq. S8). Consistently, diffusing $\cdot\text{OH}$ is not detected by ESR in COF-N32 reaction system (Fig. S42), suggests the fast oxidation process of $\cdot\text{OH}$ to H_2O_2 . Meanwhile, the introduction of tertiary butanol (TBA) has negligible effect on H_2O_2 yield by COF-N32 ($p > 0.1$), indicating that diffusing $\cdot\text{OH}$ does not have contribution to the photocatalytic process of H_2O_2 production.

In-situ FTIR spectra in sealed chamber was further employed to reveal the reactive sites on COF-N32 during the H_2O_2 generation process. The results show that H_2O adsorbed onto surfaces of COFs without light irradiation can be dissociated into $\text{C}-\text{OH}^-$ (1094 cm^{-1}) and TzH^+ (1508 cm^{-1}) in triazine rings on COF-N32 (Fig. S43)⁵⁰. To further elucidate the water oxidation process by COF-N32 with light irradiation, the in-situ FTIR spectra with the presence of O_2 and H_2O was also achieved. With the increase of reaction duration, both peaks at 1182 cm^{-1} corresponding to N-O and 1379 cm^{-1} corresponding to O-H bonds⁵¹ in COF-N32 are found to be increased. Moreover, TzH^+ (at $1522\text{--}1557\text{ cm}^{-1}$) is also generated (Figs. 5b and S44). The observation indicates that the water oxidation surrounding the N atoms in triazine rings leads to the formation of adsorbed $\cdot\text{OH}$ and H^+ . This allows the occurrence of water oxidation with relatively low overpotential of VB compared with $\text{E}(\text{H}_2\text{O}_2/\text{H}_2\text{O})$ (1.77 V vs. NHE)⁵². The production of H_2O_2 in half-reaction (with the removal of e^- by NaBrO_3) under the N_2 atmosphere (Fig. S45) confirms the presence of two-electron water oxidation process in COF-N32 reaction system, while the negligible O_2 generation in oxygen evolution experiment excluded four-electron water oxidation (Fig. S46). The isotopic experiment (using H_2^{18}O and $^{16}\text{O}_2$ as precursors in a sealed reactor) shows that the amount of $^{16}\text{O}_2$ and $^{18}\text{O}_2$ generated from the decomposition of H_2O_2 is generally equivalent (Fig. S27b), which further confirms the presence of two-electron water oxidation as well as the charge conservation with oxygen reduction during the H_2O_2 production process. It is worth pointing out that replacing triazine rings in COF-N32 by benzene rings (COF-C32) can decrease the yield of H_2O_2 under visible light irradiation (Fig. S47). The observation indicates that introduction of triazine

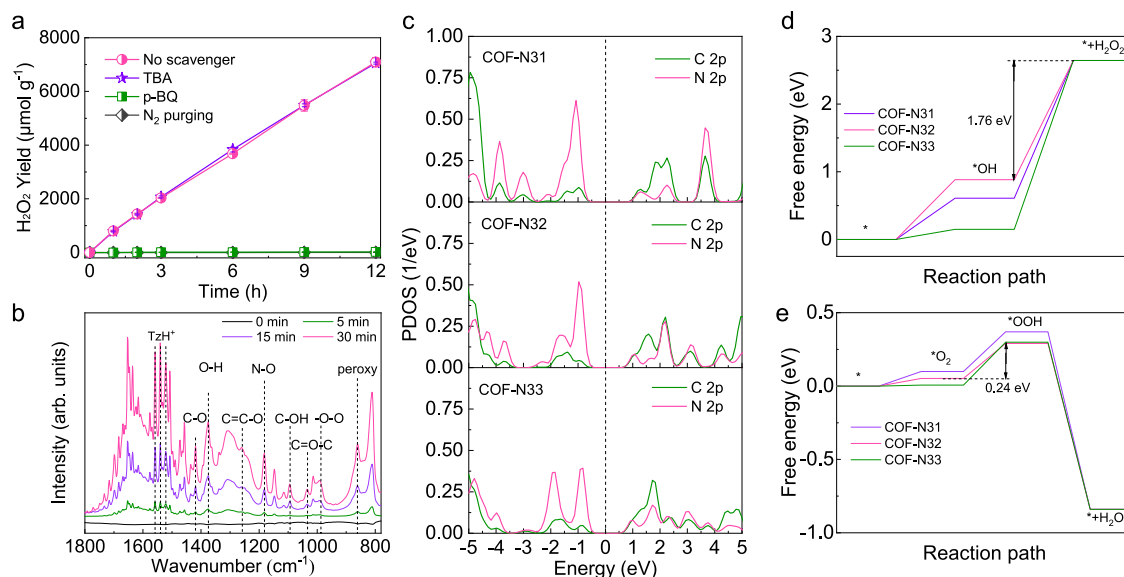


Fig. 5 | Photocatalytic mechanisms for H₂O₂ production process. **a** Quenching experiments for H₂O₂ photosynthesis. Experimental conditions: $\lambda > 420$ nm (298 K; xenon lamp, light intensity: 100 mW cm⁻²), volume (50 mL), photocatalyst (25 mg), [p-BQ]₀ = 3 mM, [TBA]₀ = 3 mM. **b** Time-course in-situ FTIR spectra of O₂ on COF-N32 under visible light irradiation with O₂. **c** PDOS of COF-N31, COF-N32 and COF-N33. The dashed lines stand for the Fermi level. Calculated energy profile for **(d)** oxidation of water into H₂O₂ and **(e)** reduction of oxygen into H₂O₂ on COF-N31, COF-N32 and COF-N33 at U = 0 V vs. SHE at pH = 7. Error bars in **a** represent the average values (mean \pm s.d., n = 3).

structure into COFs is favorable for H₂O₂ production via facilitating water oxidation. The vibration peak at 990 cm⁻¹ is corresponded to adsorbed -O₂⁻ and that at 861 cm⁻¹ is corresponded to peroxy species (-O-O-) in the in-situ FTIR spectra of COF-N32 (Figs. 5b and S48)³³. The formation of C-O (1419 cm⁻¹) and C=C-O (1264 cm⁻¹) in the in-situ FTIR spectra of COF-N32 further suggest the reduction of O₂ occurs at C atoms of COF-N32.

The H₂O₂ photosynthesis process by COFs was further revealed by theoretical calculation. The calculated PDOS plots show that the valence band top and conduction band bottom in all three COFs mainly consist of N 2p and C 2p states, respectively (Fig. 5c). This implies that during the photocatalytic reaction in all three COFs, the N sites act as the oxidizing centers, while the C sites serve as reducing centers. Comparing with COF-N31 with weakened π conjugation, the N 2p states in COF-N33 move toward a more negative region. N 2p states of COF-N32 locate between those of COF-N31 and COF-N33. Note that more negative N 2p states can easily lead to the formation of unstable chemical bond between catalyst and reactant molecule. In contrast, more positive N 2p states readily causes the formation of inert chemical bond, which is not beneficial for the catalytic reaction either⁵⁴. Instead, a moderate location of N 2p can effectively improve the photocatalytic activity. Likewise, the location of C 2p states in COF-N32 is also between those in COF-N31 and COF-N33. Hence, the H₂O₂ yield by COF-N32 is greatest among three COFs. The energy profiles of H₂O₂ production by three COFs were further determined. As shown in Fig. 5d, e, the water oxidation is the rate-determining reaction in the photocatalytic water and oxygen reforming. Moreover, the conversion of *OH into *+H₂O₂ is the rate-determining step in water oxidation⁵⁵. Specifically, COF-N32 owns a lowest energy barrier (1.76 eV) among three COFs. Meanwhile, the energy barrier of oxygen reduction into H₂O₂ by COF-N32 is only 0.24 eV, which is also the lowest among COFs. Hence, the highest H₂O₂ yield is obtained by COF-N32 with light irradiation.

In summary, in order to enhance the yield of H₂O₂ by COFs under light irradiation, we propose a strategy to facilitate the formation and dissociation of excitons in COFs through optimizing the intramolecular polarity of COFs by introducing suitable amount of phenyl group as electron donors. We fabricate a class of COFs with different intramolecular polarity by using triazine-cored triamine with different

amount of phenyl group ($n=0, 1, 2$) as the precursors. We find that among all three COFs, COF-N32 with moderate intramolecular polarity in the octupolar conjugated structure can generate greatest amount of charges (i.e. electrons) for H₂O₂ photosynthesis under light irradiation. Without the requirement of sacrificial agent, the H₂O₂ yield by COF-N32 reaches 7092 $\mu\text{mol g}^{-1}$ (605 $\mu\text{mol g}^{-1} \text{h}^{-1}$) after 12 h of visible light irradiation with solar-to-chemical efficiency of 0.31% and high AQY of 6.2% at 459 nm. Moreover, we find that COF-N32 can also efficiently produce H₂O₂ in more available real water samples including tap water, river water and sea water. COF-N32 can be assembled into practical devices for consecutive uses with high photocatalytic stability. COF-N32 either dispersed in membrane filter reactors or immobilized onto glass slides can efficiently produce H₂O₂ under natural sunlight irradiation. During the H₂O₂ photosynthesis process, suitable N 2p states and C 2p states in COF-N32 with optimal intramolecular polarity reduce the energy barrier for H₂O activation and oxygen reduction, respectively, contributing to the high efficiency. This study not only provides deep insight into the design of COFs via regulating its intramolecular polarity to boost the H₂O₂ photosynthesis without using sacrificial agent, but also paves the way for the practical application of COFs-based photosynthesis of H₂O₂.

Methods

COFs synthesis

Unlike COF-N32 and COF-N33 that can be fabricated by using one-pot solvothermal method based on the Schiff-base reaction between two types of precursors in mesitylene/dioxane/acetic acid solvent, COF-N31 yet can not be successfully synthesized by the mixture of 1,3,5-triformylphloroglucinol (Tp) and melamine in mesitylene/dioxane/acetic acid solvent due to its instability in this solvent. Instead, COF-N31 were fabricated in dimethyl sulfoxide/*N,N*-dimethylacetamide (DMAc)/acetic acid following the method reported in previous literature²². Specifically, 0.3 mmol of Tp (63 mg) and 0.3 mmol of melamine (38 mg) were added into a reactor, followed by the addition of 2 mL of dimethyl sulfoxide, 1 mL of DMAc and 0.3 mL of 6 M acetic acid. After ultrasonication and degassed by three consecutive freeze-pump-thaw cycles, the reactor was sealed under vacuum condition,

which was then heated at 120 °C for 72 h. The collected product was firstly rinsed by DMAc, which was then solvent exchanged with DMAc, pure water and washed with acetone for three times. The final product was dried at 120 °C under vacuum.

COF-N32 and COF-N33 were synthesized by mixing Tp with the precursors with triazine and triamine in mesitylene/dioxane/acetic acid solvent, respectively. Briefly, 0.9 mmol (190 mg) of Tp and 0.9 mmol of 4,4',4''-(1,3,5-triazine-2,4,6-triyl)-trianiline (318.6 mg, for COF-N32) or 4,4',4''-(1,3,5-triazine-2,4,6-triyl)tris([1,1'-biphenyl]-4-amine) (524 mg, for COF-N33) were added into a Teflon lining with the volume of 20 mL. Then, dioxane (4.5 mL), mesitylene (4.5 mL) and 3 M acetic acid (1.5 mL) were added. The mixture was ultrasonicated and bubbled with N₂ for 20 min. After that, the Teflon lining was sealed in an autoclave and heated at 120 °C in the oven for 72 h. The mixture was separated through filtration and the solid was rinsed by acetone for five times, which was finally dried at 60 °C. The precursors-to-COFs efficiency is 76% for COF-N31, 78% for COF-N32 and 75% for COF-N33, respectively.

Photocatalytic experiments

The photosynthesis of H₂O₂ was first performed in a double wall quartz reactor with 50 mL of ultrapure water and 25 mg of photocatalysts (1, 5 and 10 mg of COF-N32 were also considered in particular experiments). The initial solution pH of the mixture was adjusted by NaOH or HClO₄. The reaction suspension was irradiated by using a 300 W Xenon lamp ($\lambda > 420$ nm, 100 ± 1 mW cm⁻²). The temperature was fixed at 25.0 ± 0.2 °C by circulating water system during the photocatalytic experiments. The reaction suspension was extracted and filtered for H₂O₂ measurement at specific time intervals. The reusability of three COFs was investigated. The H₂O₂ production by COF-N32 in various real waters (e.g. tap water, river water and sea water) was evaluated under both simulated visible light and natural solar light. COF-N32 were employed in commercial membrane reactors and further immobilized onto ITO glass with the size of 10 cm × 10 cm for the continuous H₂O₂ photosynthesis.

Catalyst characterization

XRD (DMAX-2400, Rigaku, Japan), XPS (Axis Ultra, Kratos, UK), SEM (JSM-F100, JEOL, Japan), TEM (Tecnai F30, USA), ¹³C NMR (Bruker-400 AVANCE III, Bruker, Switzerland), FTIR (Nicolet is50, Thermo Fisher, USA) were employed to reveal the chemical and structural information of COFs. In-situ FTIR spectra measurement (Bruker Tensor, Bruker, Switzerland), UV-vis DRS (UV-2400, Shimadzu, Japan), steady state PL spectra, time-resolved PL decay curve, temperature-dependent PL spectra (FLS980, Edinburgh, UK), TA spectrometer (Helios, Ultrafast System, USA), ESR analysis (Bruker EMX, Bruker, Switzerland), water adsorption analysis (3Flex, Micromeritics, USA), RRDE (PINE E6, USA), ¹⁸O isotopic experiment and EIS (CHI760E, Chenhua, China) were performed to investigate the mechanisms of H₂O₂ photosynthesis by prepared COFs.

Data availability

The data that support the findings of this study are available within the article and its Supplementary Information. Source data are provided with this paper.

References

- Xia, C., Kim, J. Y. & Wang, H. Recommended practice to report selectivity in electrochemical synthesis of H₂O₂. *Nat. Catal.* **3**, 605–607 (2020).
- Perry, S. C. et al. Electrochemical synthesis of hydrogen peroxide from water and oxygen. *Nat. Rev. Chem.* **3**, 442–458 (2019).
- Richards, T. et al. A residue-free approach to water disinfection using catalytic in situ generation of reactive oxygen species. *Nat. Catal.* **4**, 575–585 (2021).
- Xia, C., Xia, Y., Zhu, P., Fan, L. & Wang, H. Direct electrosynthesis of pure aqueous H₂O₂ solutions up to 20% by weight using a solid electrolyte. *Science* **366**, 226–231 (2019).
- Campos-Martin, J. M., Blanco-Brieva, G. & Fierro, J. L. G. Hydrogen peroxide synthesis: an outlook beyond the anthraquinone Process. *Angew. Chem. Int. Ed.* **45**, 6962–6984 (2006).
- Hou, H., Zeng, X. & Zhang, X. Production of hydrogen peroxide by photocatalytic processes. *Angew. Chem. Int. Ed.* **59**, 17356–17376 (2020).
- He, B. et al. Cooperative coupling of H₂O₂ production and organic synthesis over a floatable polystyrene-sphere-supported TiO₂/Bi₂O₃ S-scheme photocatalyst. *Adv. Mater.* **34**, 2203225 (2022).
- Teng, Z. et al. Atomically dispersed antimony on carbon nitride for the artificial photosynthesis of hydrogen peroxide. *Nat. Catal.* **4**, 374–384 (2021).
- Chu, C. et al. Spatially separating redox centers on 2D carbon nitride with cobalt single atom for photocatalytic H₂O₂ production. *Proc. Natl. Acad. Sci.* **117**, 6376–6382 (2020).
- Tian, Z. et al. Efficient photocatalytic hydrogen peroxide generation coupled with selective benzylamine oxidation over defective ZrS₃ nanobelts. *Nat. Commun.* **12**, 2039 (2021).
- Xu, X. et al. Conjugated Organic Polymers with Anthraquinone Redox Centers for Efficient Photocatalytic Hydrogen Peroxide Production from Water and Oxygen under Visible Light Irradiation without Any Additives. *ACS Catal.* **12**, 12954–12963 (2022).
- Xu, X. et al. The construction of conjugated organic polymers containing phenanthrenequinone redox centers for visible-light-driven H₂O₂ production from H₂O and O₂ without any additives. *Chem. Eng. J.* **454**, 139929 (2023).
- Krishnaraj, C. et al. Strongly reducing (diarylamino)benzene-based covalent organic framework for metal-free visible light photocatalytic H₂O₂ generation. *J. Am. Chem. Soc.* **142**, 20107–20116 (2020).
- Wang, H., Yang, C., Chen, F., Zheng, G. & Han, Q. A Crystalline Partially Fluorinated Triazine Covalent Organic Framework for Efficient Photosynthesis of Hydrogen Peroxide. *Angew. Chem. Int. Ed.* **61**, e202202328 (2022).
- Kim, T. W. et al. Ultrafast charge transfer coupled with lattice phonons in two-dimensional covalent organic frameworks. *Nat. Commun.* **10**, 1873 (2019).
- Clarke, T. M. & Durrant, J. R. Charge Photogeneration in Organic Solar Cells. *Chem. Rev.* **110**, 6736–6767 (2010).
- Zhang, M. et al. Semiconductor/covalent-organic-framework Z-scheme heterojunctions for artificial photosynthesis. *Angew. Chem. Int. Ed.* **59**, 6500–6506 (2020).
- Wang, P., Zhao, D. & Yin, L. Two-dimensional matrices confining metal single atoms with enhanced electrochemical reaction kinetics for energy storage applications. *Energy Environ. Sci.* **14**, 1794–1834 (2021).
- Dey, K., Kunjattu, H. S., Chahande, A. M. & Banerjee, R. Nanoparticle size-fractionation through self-standing porous covalent organic framework films. *Angew. Chem. Int. Ed.* **59**, 1161–1165 (2020).
- Kandambeth, S. et al. Construction of crystalline 2D covalent organic frameworks with remarkable chemical (acid/base) stability via a combined reversible and irreversible route. *J. Am. Chem. Soc.* **134**, 19524–19527 (2012).
- Dey, K. et al. Selective Molecular Separation by Interfacially Crystallized Covalent Organic Framework Thin Films. *J. Am. Chem. Soc.* **139**, 13083–13091 (2017).
- Bhadra, M. et al. Triazine Functionalized Porous Covalent Organic Framework for Photo-organocatalytic E-Z Isomerization of Olefins. *J. Am. Chem. Soc.* **141**, 6152–6156 (2019).
- Ye, Y.-X. et al. A solar-to-chemical conversion efficiency up to 0.26% achieved in ambient conditions. *Proc. Natl. Acad. Sci.* **118**, e2115666118 (2021).

24. Gu, S. et al. Tunable redox chemistry and stability of radical intermediates in 2D covalent organic frameworks for high performance sodium ion batteries. *J. Am. Chem. Soc.* **141**, 9623–9628 (2019).
25. Lu, T. & Chen, F. Multiwfn: A multifunctional wavefunction analyzer. *J. Comput. Chem.* **33**, 580–592 (2012).
26. Thalladi, V. R. et al. Crystal engineering of some 2,4,6-triaryloxy-1,3,5-triazines: octupolar nonlinear materials. *J. Am. Chem. Soc.* **120**, 2563–2577 (1998).
27. Xu, J. et al. Vinylene-linked covalent organic frameworks (COFs) with symmetry-tuned polarity and photocatalytic activity. *Angew. Chem. Int. Ed.* **59**, 23845–23853 (2020).
28. Lan, Z.-A., Fang, Y., Zhang, Y. & Wang, X. Photocatalytic oxygen evolution from functional triazine-based polymers with tunable band structures. *Angew. Chem. Int. Ed.* **57**, 470–474 (2018).
29. Liao, Y., Wang, H., Zhu, M. & Thomas, A. Efficient supercapacitor energy storage using conjugated microporous polymer networks synthesized from Buchwald–Hartwig coupling. *Adv. Mater.* **30**, 1705710 (2018).
30. Guo, L., Niu, Y., Razaque, S., Tan, B. & Jin, S. Design of D–A1–A2 Covalent Triazine Frameworks via Copolymerization for Photocatalytic Hydrogen Evolution. *ACS Catal.* **9**, 9438–9445 (2019).
31. Pagidi, S., Kalluvettukuzhy, N. K. & Thilagar, P. Effect of branching on the delayed fluorescence and phosphorescence of simple borolated arylamines. *Inorg. Chem.* **59**, 3142–3151 (2020).
32. Haug, W. K., Moscarello, E. M., Wolfson, E. R. & McGrier, P. L. The luminescent and photophysical properties of covalent organic frameworks. *Chem. Soc. Rev.* **49**, 839–864 (2020).
33. Li, X. et al. Facile transformation of imine covalent organic frameworks into ultrastable crystalline porous aromatic frameworks. *Nat. Commun.* **9**, 2998 (2018).
34. Jin, E. et al. Two-dimensional sp^2 carbon-conjugated covalent organic frameworks. *Science* **357**, 673–676 (2017).
35. Bi, S. et al. Two-dimensional semiconducting covalent organic frameworks via condensation at arylmethyl carbon atoms. *Nat. Commun.* **10**, 2467 (2019).
36. Hamlin, T. A., Bickelhaupt, F. M. & Fernández, I. The Pauli repulsion-Lowering concept in Catalysis. *Acc. Chem. Res.* **54**, 1972–1981 (2021).
37. Yao, L. et al. Highly efficient near-infrared organic light-emitting diode based on a butterfly-shaped donor–acceptor chromophore with strong solid-state fluorescence and a large proportion of radiative excitons. *Angew. Chem. Int. Ed.* **53**, 2119–2123 (2014).
38. Li, Y. et al. In situ photodeposition of platinum clusters on a covalent organic framework for photocatalytic hydrogen production. *Nat. Commun.* **13**, 1355 (2022).
39. Yuan, M. et al. Deuterated covalent organic frameworks with significantly enhanced luminescence. *Angew. Chem. Int. Ed.* **60**, 21250–21255 (2021).
40. Huang, N., Ding, X., Kim, J., Ihee, H. & Jiang, D. A photoresponsive smart covalent organic framework. *Angew. Chem. Int. Ed.* **54**, 8704–8707 (2015).
41. Ran, L. et al. Engineering single-atom active sites on covalent organic frameworks for boosting CO_2 photoreduction. *J. Am. Chem. Soc.* **144**, 17097–17109 (2022).
42. Yang, W. et al. Electron accumulation induces efficiency bottleneck for hydrogen production in carbon nitride photocatalysts. *J. Am. Chem. Soc.* **141**, 11219–11229 (2019).
43. Fang, X. et al. Single Pt atoms confined into a metal–organic framework for efficient photocatalysis. *Adv. Mater.* **30**, 1705112 (2018).
44. Shiraishi, Y. et al. Resorcinol–formaldehyde resins as metal-free semiconductor photocatalysts for solar-to-hydrogen peroxide energy conversion. *Nat. Mater.* **18**, 985–993 (2019).
45. Liu, L. et al. Linear conjugated polymers for solar-driven hydrogen peroxide production: the importance of catalyst stability. *J. Am. Chem. Soc.* **143**, 19287–19293 (2021).
46. Zhao, W. et al. Accelerated synthesis and discovery of covalent organic framework photocatalysts for hydrogen peroxide production. *J. Am. Chem. Soc.* **144**, 9902–9909 (2022).
47. Zhu, L. et al. Designing 3D– MoS_2 sponge as excellent cocatalysts in advanced oxidation processes for pollutant control. *Angew. Chem. Int. Ed.* **59**, 13968–13976 (2020).
48. Wu, Q. et al. A metal-free photocatalyst for highly efficient hydrogen peroxide photoproduction in real seawater. *Nat. Commun.* **12**, 483 (2021).
49. Gopakumar, A. et al. Lignin-supported heterogeneous photocatalyst for the direct generation of H_2O_2 from seawater. *J. Am. Chem. Soc.* **144**, 2603–2613 (2022).
50. Dunwell, M., Yan, Y. & Xu, B. In situ infrared spectroscopic investigations of pyridine-mediated CO_2 reduction on Pt electrocatalysts. *ACS Catal.* **7**, 5410–5419 (2017).
51. Kou, M. et al. Molecularly engineered covalent organic frameworks for hydrogen peroxide photosynthesis. *Angew. Chem. Int. Ed.* **61**, e202200413 (2022).
52. Cheng, H. et al. Rational design of covalent heptazine frameworks with spatially separated redox centers for high-efficiency photocatalytic hydrogen peroxide production. *Adv. Mater.* **34**, 2107480 (2022).
53. Zhang, M., de Respinis, M. & Frei, H. Time-resolved observations of water oxidation intermediates on a cobalt oxide nanoparticle catalyst. *Nat. Chem.* **6**, 362–367 (2014).
54. Zhou, P. et al. Single-atom Pt– I_3 sites on all-inorganic Cs_2SnI_6 perovskite for efficient photocatalytic hydrogen production. *Nat. Commun.* **12**, 4412 (2021).
55. Chen, L. et al. Acetylene and diacetylene functionalized covalent triazine frameworks as metal-free photocatalysts for hydrogen peroxide production: a new two-electron water oxidation pathway. *Adv. Mater.* **32**, e1904433 (2020).

Acknowledgements

This work was supported by Fund for Innovative Research Group of NSFC under Grant No. 51721006 and the National Natural Science Foundation of China under Grant No. 42025706 and 52270015.

Author contributions

M.P.T. and F.Y.L. designed the research. F.Y.L. and P.Z. performed the research with the help of Y.H.H., H.T., and Y.L. F.Y.L., P.Z. and M.P.T. wrote the paper. J.L.L., Q.Z. S.J.G and J.R.N. provided ideas. All the co-authors contributed to interpretation of the findings.

Competing interests

The authors declare no competing interests.

Additional information

Supplementary information The online version contains supplementary material available at <https://doi.org/10.1038/s41467-023-40007-4>.

Correspondence and requests for materials should be addressed to Meiping Tong.

Peer review information *Nature Communications* thanks Hong Zhong and the other anonymous reviewer(s) for their contribution to the peer review of this work. A peer review file is available.

Reprints and permissions information is available at <http://www.nature.com/reprints>

Publisher's note Springer Nature remains neutral with regard to jurisdictional claims in published maps and institutional affiliations.

Open Access This article is licensed under a Creative Commons Attribution 4.0 International License, which permits use, sharing, adaptation, distribution and reproduction in any medium or format, as long as you give appropriate credit to the original author(s) and the source, provide a link to the Creative Commons license, and indicate if changes were made. The images or other third party material in this article are included in the article's Creative Commons license, unless indicated otherwise in a credit line to the material. If material is not included in the article's Creative Commons license and your intended use is not permitted by statutory regulation or exceeds the permitted use, you will need to obtain permission directly from the copyright holder. To view a copy of this license, visit <http://creativecommons.org/licenses/by/4.0/>.

© The Author(s) 2023